# Complementary characterization method of 3D arsenic doping by using medium energy ion scattering

L Penlap Woguia, F Pierre, D F Sanchez, G G Marmitt, Z Saghi, D Jalabert

IOP Publishing J. Phys. Commun. 5 (2021) 015017 https://doi.org/10.1088/2399-6528/abbdcf

Journal of Physics Communications

PAPER

# Complementary characterization method of 3D arsenic doping by using medium energy ion scattering

L Penlap Woguia[1], F Pierre[1], D F Sanchez[2], G G Marmitt[3], Z Saghi[1] and D Jalabert[4]

[1] Univ. Grenoble Alpes, CEA, LETI, F-38000 Grenoble, France
[2] Paul Scherrer Institut, WLGA/221, CH-5232, Villigen PSI, Switzerland
[3] Department of Radiation Oncology, Universitair Medisch Centrum Groningen, Hanzeplein 1, 9713 GZ, Netherlands
[4] Univ. Grenoble Alpes, CEA, DRF, IRIG, F-38000 Grenoble, France

E-mail: lucien.p.woguia@aims-senegal.org

OPEN ACCESS

RECEIVED
12 September 2020

REVISED
30 September 2020

ACCEPTED FOR PUBLICATION
2 October 2020

PUBLISHED
22 January 2021

Keywords: 3D-MEIS, 3D-doping, experimental protocol, PowerMEIS simulation, FinFET, SOI



## Abstract

We report on a new characterization method of 3D—doping performed by arsenic implantation into FinFET—like nanostructures by using Medium Energy Ion Scattering. Because of its good depth resolution (0.25 nm) at the surface, it is one of techniques of choice suitable to analyse the ultra-shallow doping of thin crystal films. However, with the constraints related to the nanostructures' geometry and the low lateral resolution of the MEIS beam (0.5 × 1 $mm^2$), we developed an adequate protocol allowing their analysis with this technique. It encompasses three different geometries to account for the MEIS spectra of the arsenic implanted in each part of the nanostructures. The originality of the protocol is that, according to the chosen analysis geometry, the overall spectrum of arsenic is not the same because the contributions of each part of the patterns to its formation are different. By using two of them, we observed double peaks of arsenic. Thanks to 3D deconvolutions performed with PowerMEIS simulations, we were able to identify the contribution of the tops, sidewalls and bottoms in their formation. Thus, by separating the spectrum of the dopants implanted in the Fins (tops + sidewalls) from that of the bottoms, we were able to characterize the 3D doping conformity in the patterns. Two different implantation methods with the associated local doses computed in each single part were investigated. We found that the distribution of the dopants implanted by using the conventional implanter method is very different from that of plasma doping.

## 1. Introduction

The three dimensional (3D) Fin Field Effect Transistor (FinFET) stands as one of the most efficient solutions adopted by the microelectronic industry to circumvent the issues encountered with the miniaturization of planar (2D) MOSFETs. Doping being one of the key steps in their fabrication procedures, the advent of nanostructures of non planar architectures makes it highly challenging. Not only because of the shape, size and structure dependency [1], but also the distribution of the implants in all the parts which should be uniform. It can be performed by using several techniques as reported in the literature [2]. However, the low manufacturing cost of semiconductors (SCs) devices requires cheap doping methods.

Ion implantation is known as the most used technique for introducing foreign atoms inside SCs. Doping can be achieved by using the conventional Implanter (IM) and Plasma Immersion Ion Implantation (PIII) methods. The former is widely utilised because of its good energy control of the dopants. However, the unidirectionality of the ion beam obliges to perform the implantation into 3D-Fin shaped nanostructures in many steps, which is costly and time consuming. Because of the large throughput and multidirectional implantation that it affords, PIII is a good alternative for the doping of non planar structures in only a single step [2]. The sample is actually immersed into a chamber where the positive, negative and neutral charges generated by a plasma gas strike its surface. By exploiting the multiple collision cascades between the particles, one can expect a large scale 3D doping and their uniform distribution within the patterns.

Table 1. Description of the investigated samples. The doping methods as well as the other parameters are indicated. The twist(°) is the rotation angle of the wafer around itself and tilt(°) is the inclination angle off its surface normal so as to optimise the sidewalls doping. The implantation has been performed at room temperature (RT). The targeted doses were $1 \times 10^{15}$ at $cm^{-2}$ and $5 \times 10^{15}$ at $cm^{-2}$ for the implanter and plasma methods, respectively.

| Samples | Doping methods | Species | Energy(keV) | Tilt(°) | Twist(°) | Temperature(°C) |
|---|---|---|---|---|---|---|
| S1 | Implanter | As | 3 keV | 25 | 180 | RT |
| S2 | Plasma | $AsH_3$ | 3 keV | — | — | RT |

The objective of this work is to study the doping conformity and quantify arsenic ($As^+$) implanted by using the two above mentioned methods into nanostructures elaborated from silicon on insulator (SOI) materials. The local dose really received by the patterns can readily be measured by using Medium Energy Ion Scattering (MEIS). Because the outcomes are not altered by the matrix effects or sputtering induced re-implantation as it is often the case in Secondary Ion Mass Spectrometry (SIMS) [3, 4]. MEIS was already used in previous works to analyse 3D plasma or conventional arsenic doping into Si nanostructures [3, 5, 6]. Alongside the quantification of As in both the planar and non-planar SOI samples, our studies are focused on the doping conformity in the nanostructured ones implanted by using the two methods. In the other words, we will check if the distribution of dopants in the tops, sidewalls and bottoms (oxide) is the same in the IM and PIII methods. Indeed, if the process looks more predictable in IM, it is not obvious in PIII because of mass selection and many other parameters to control such as pressure, high throughput, fluence, etc. The outcomes may therefore not be as expected with this latter implantation method. The final results can actually yield to non equivalent distributions of dopants in the tops, sidewalls and oxide. The analysis method should also afford better investigation of the difficultly accessible parts such as sidewalls and bottoms. Hence the experimental protocol presented below, has been developed in order to access to all these information.

## 2. Experimental methods

### 2.1. Samples and techniques

The patterns were formed by electron beam (e-beam) lithography and chlorine based dry etching on SOI based wafers of 300 mm diameter. The nanometric silicon (Si) lines grating (Fins) are of 1.2 mm long, 59–60 nm height with the periodicity (pitch) of 160 nm, etched on a 25 nm thick oxide ($SiO_2$) with widths of 43 nm and 46 nm. They stand as model structures dedicated to FinFET channels without applied electrodes. The implantation parameters are presented in table 1.

It is known that $As^+$ is utilised for n-type doping because of its high solid solubility [7, 8] and shallow penetration [9]. In this work, the conventional implantation was performed by using $As^+$ on a VIISTA HCP setup at 3 keV in the conditions as indicated in table 1. A two steps process was required in order to implant the sidewalls at an incidence angle of 25°. The PIII doping was carried out on a PULSION® Nano tool manufactured by Ion Beam Services (IBS) by using arsine ($AsH_3^+$) gas. The sample was mounted on a holder (chunk), negatively pulse biased at 3 kV during the implantation. The temperature within the chamber was the same as that in the former method and the doping achieved at high pressure ($10^{-2}$ mbar) so as to reduce the ion mean free path [10].

MEIS is a technique capable to provide structural and compositional information upon a sample. It consists in analysing the energy or angle of the projectiles scattered from the sample from which an elemental composition can be investigated. Structural information (e.g. interstitials) can be obtained when the incident beam is aligned with a major crystallographic axis. A good quantification is achieved with this technique when the beam is randomly oriented onto the crystal, so that a significant fraction of the incident projectiles is more likely to see all the atoms and give rise to a high scattered yield in the energy spectrum. Hence one can determine substitutional fractions and thereby activated atoms [11–13]. The MEIS experiments were carried out in random orientation with an electrostatic accelerator that can generate a proton ($H^+$) beam of 200 keV energy. During the measurements, the sample is mounted on a high precision three axis goniometer fixed at the center of an ultra high vacuum (UHV) analyzing chamber. The experiments were performed at the incidence angle of 64° and normal incidence with respect to the samples' surface. The scattered ions were analysed in energy at the respective scattering angles of 119° (for normal incidence) and 135° (for 64° incidence) by a toroidal electrostatic analyser (TEA). The high energy and angular resolutions obtainable with this detection system are about $(\Delta E/E) = 3.3 \times 10^{-3}$ and 0.1°, respectively.

A thin lamella was prepared for electron microscopy by focused ion beam (FIB) milling and analyzed in an FEI Titan Themis operating at 200 kV and equipped with a probe corrector and 4 SDD EDX detectors. High

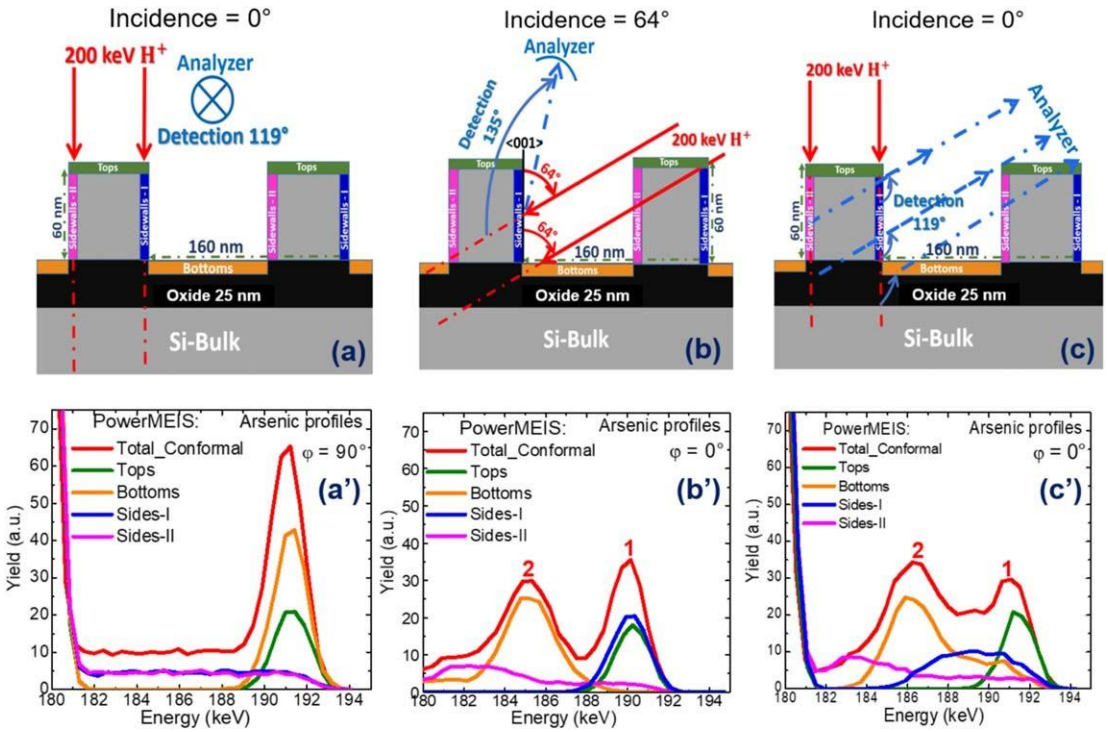


Figure 1. Schematic illustration of the three geometries of the analysis protocol and their corresponding PowerMEIS [14, 15] simulations. They depict the MEIS spectra of the arsenic implanted in the tops, sidewalls I and II and the bottoms surfaces. (a) and (a'): analysis in normal incidence with the scattered projectiles exiting longitudinally with respect to the Fins. (b) and (b'): analysis in inclined incidence where the scattered projectiles exit laterally with respect to the Fins as well. In graphs (c) and (c'), the lines grating have the same orientation like in (b) and (b') but they are analysed in normal incidence. The azimuth (j = 90° and 0°) is their orientation in the plane of the sample.

angle annular dark field—scanning transmission electron microscopy images gave access to morphological information related to the Fins and EDX was used for elemental mapping (figure 7).

## 2.2. Analysis protocol

The size of the beam delivered by the MEIS equipment (1 × 0.5 $mm^2$) is by far larger than the dimensions of the patterns. Several orientations of the Fins were therefore explored to determine the MEIS spectra of arsenic implanted within their structure. The idea is to use different incidence angles to separate the spectra of the tops, sidewalls and bottoms so that they do not appear at the same energy positions. The three geometries that we need to achieve this are presented in figure 1 with their associated MEIS spectra simulated with PowerMEIS [14, 15]. Similar analyses were performed in [5] by using the same tool where three other geometries were considered to investigate only conventional implantation into full Si line gratings. PowerMEIS is a software that uses Monte-Carlo methods to calculate all the trajectories of ions into 3D structures of any geometrical shape. The approach used for the modelling is similar to that described in litterature [5, 16, 17]. Indeed, the nanostructures to simulate are discretised into several 3D matrix layers of defined densities (2.33g $cm^{-3}$ for Si and 2.32 g $cm^{-3}$ for $SiO_2$), stoichiometry, composition of various atomic percentage of As and thickness in nm.

The example model adopted for the simulations in this protocol was of SOI type, considered as conformally doped with the patterns of 60 nm height, 44 nm width and periodicity = 160 nm. We define an implantation as conformal when the tops, sidewalls and bottoms have received the same dose per $cm^{-2}$. The model matrix used for PowerMEIS simulations of a conformal implantation is presented in figure 2. The total number of layers implanted with As introduced at each part are the same (10) and of equal thicknesses. The As concentration varies from the layers much closer to the surface to the deeper ones, but in the same proportions for the tops, sidewalls and bottoms. However, for a non conformal implantation, only the As concentration was varied in different proportions in each layer so that those with null concentrations do not contribute in the local dose quantification at the corresponding part of the patterns.

By simulating the MEIS spectrum of arsenic with the geometry of figure 1(a), the result is as presented in figure 1(a'). One observes only a single arsenic peak. Thanks to the 3D deconvolutions that we developed, we show that the spectra of the tops and bottoms overlap at the same energy position in figure 1(a'). However, the signal of the two sidewalls are discriminated from the others. It can be seen that the contribution of the two sidewalls (I and II) are equivalent. By adopting this hypothesis in the second geometry (figure 1(b)), the

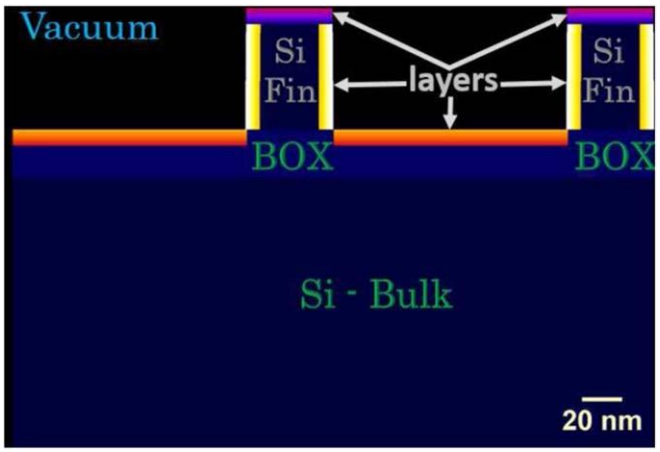


Figure 2. Representation of the matrix model used for PowerMEIS simulations of a conformal implantation. It shows the Si-Fins and Si-bulk separated by a buried oxide (BOX). The layers illustrate the implantation of As at each part, they are assumed to have the same thickness but different stoichiometries.

simulated spectrum of arsenic in figure 1(b') diplays two peaks 1 and 2. The peak 1 emanates from the contribution of Si-Fins (tops + sidewalls) and peak 2 is for the oxide (bottoms). However, it is shifted towards the lower energy range because of the incidence and scattering angles. The incidence of 64° was actually chosen such that the 200 keV $H^+$ projectiles cross the patterns and loose energy before interacting with the arsenic atoms implanted in the oxide. Which also explains why the signal of the arsenic implanted in sidewalls—II appears flattened along the energy axis in figure 1(b'). If one maintains this orientation of the patterns as in figure 1(b) (azimuth $j = 0°$) and probe them in normal incidence (see figure 1(c)), the results are as presented in figure 1(c'), which is the third geometry. There is an energy region (~188–191 keV) in figure 1(c') where the contributions of the four parts superimpose. Nevertheless, the spectrum of the bottoms is still discriminated from the others because the scattered $H^+$ undergo supplementary energy losses when they exit the patterns at the scattering angle of 119°. When the incident $H^+$ cross the patterns along their 60 nm height, they considerably loose energy. An important fraction of the scattered projectiles experience additional energy losses when they exit the patterns and cross the neighboring Fins. This explains the shape of the simulated spectra of sidewalls—I and II in figure 1(c'). Indeed, the importance of this third geometry is that it helps verify the second one (figures 1(b) and (b')) precisely the doping of the two sidewalls. Let us suppose that one omits the contribution of sidewalls—II in the model. With the second geometry, one can still fit the overall spectrum of arsenic by relying on the spectra of the bottoms and sidewalls—I. However, this does no longer hold in the third geometry because figure 1(c') shows that one obligatorily needs the spectrum of sidewalls—II to account for the overall spectrum of arsenic. With this original method of investigating 3D doping with MEIS, we show that three geometries are sufficient to reconstruct the spectrum of the implants. The experimental results are commented in the following sections.

## 3. Results and discussions

### 3.1. Preliminary measurements on planar structures

The quantification of the dopants implanted in the planar structures (non-etched areas) has been performed by MEIS on the two samples, then verified by Rutherford Backscattering Spectrometry (RBS). It is known as a technique of reference for elemental quantification into solid matrices [11, 12], because of its good capability of counting the ions of different charge states (positive, negative and neutrals) scattered from their structures. It was even demonstrated that this technique was able to investigate the As composition into complex nanostructures [18]. The RBS analyses were carried out in random orientation with 2 MeV alphas projectiles on the same samples, striking their surfaces at an incidence angle of 62°. The scattered projectiles were analysed at a scattering angle of 160°. The spectra (not shown) were simulated with SIMNRA [19]. The doses of arsenic were computed by simulating the MEIS spectra (figure 3) by using the MEISanalyser.exe software developed by Denis Jalabert. The electrostatic detection system used in MEIS is only capable to detect charged projectiles. For accuracy in the calculations, the fraction of the singly charged ions exiting the sample has been taken into consideration, based on the work of Zalm *et al* [20]. According to table 2, one can say that the dose implanted in S1 by using the implanter method is as targeted. The discrepancy between the measured and targeted ones in S2, verified by the two experimental techniques, can be explained by the complex interactions between neutral

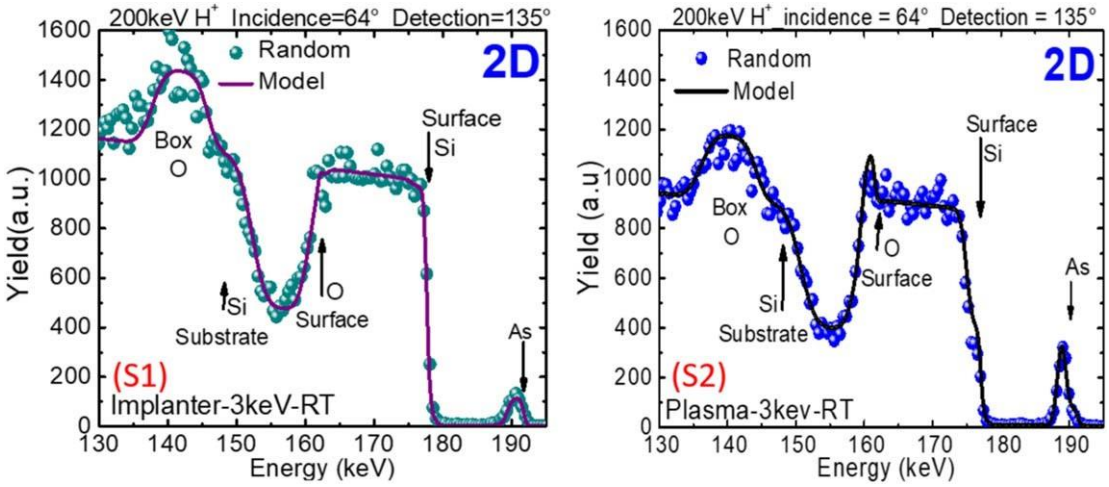


Figure 3. MEIS spectra measured on the planar samples implanted with arsenic ($As^+$ - S1) and arsine ($AsH_3^+$ - S2) with their associated fits. The incidence and scattering angles were 64° and 135°, respectively. The implantation methods are indicated in each graph.

Table 2. Comparison of the implanted doses of arsenic measured in planar (2D) structures by the two indicated techniques. The values obtained with MEIS were computed through the simulations of the experimental spectra with the respective densities: 6.9 × $10^{22}$ mol $cm^{-3}$ (for $Si_{0.36}O_{0.64}$), 2.3 × $10^{22}$ mol $cm^{-3}$ (for $SiO_2$) and 5 × $10^{22}$ mol $cm^{-3}$ (for Si). The implantation temperature and energy are recalled.

| Arsenic doses (×$10^{15}$at $cm^{-2}$): 2D Samples | | | |
|---|---|---|---|
| | Experimental techniques: | | |
| 3 keV—RT | Targeted | RBS | MEIS |
| Implanter (S1) | 1 | 0.9 ± 0.1 | 1 ± 0.04 |
| Plasma (S2) | 5 | 1.95 ± 0.5 | 2.1 ± 0.04 |

species and energeticions, with the contribution of non selection in mass in the PIII process [17, 21, 22]. Table 2 therefore shows that MEIS can be as quantitative as RBS and the obtained values have been exploited in the investigation of nanostructured samples.

### 3.2. Measurements on 3D structures

The MEIS experimental spectra measured on 3D samples in the geometries of figures (1(b) and (b') and (c) and (c')) are presented in figures 4(A) and (C) for the incidence at 64° - detection at 135° and figures 4(B) and (D) for normal incidence—detection at 119°. Unlike the arsenic spectra measured on the non etched areas of the same wafers which show only a single peak, those measured on the patterned areas display two peaks. Figure 4 also illustrates that the lines grating influence the spectrum of the overall matrix, as observed from the Si-surface edge until the lower energy range. There is an impact of the patterned structures on the outcomes that should not be underestimated. Therefore, a good geometry should be designed prior to carry out precise investigations. As depicted by the insets of figure 4, the experiments have verified the double peaks of arsenic predicted by simulations. The intensities of the two arsenic peaks in S1 (implanter) are nearly similar, but by far different from those of S2. In plasma, the yield of the first peak is higher than that of the second one, it indicates that the distribution of the implants in the two doping methods is different. For a good conformity assessment, further analyses have been performed in order to understand how the tops, bottoms and the two sidewalls participate in the formation of the two peaks.

Figures 5 and 6 show the 3D deconvolutions of the overall arsenic spectra in S1 and S2. The peaks 1 in the experimental spectra actually result from the contribution of the tops and sidewalls, while the bottoms majoritarily contribute in peaks 2. In figure 5 (sample S1), the As signal of the tops is higher than that of sidewalls, signifiying that the doping of these parts is not strictly conformal. However, the significant discrepancies with the spectra of sample S2 is readily noticeable. In plasma, the tops are the most dominant in peak 1 comparatively to the sidewalls. The arsenic's peak of the bottoms is ~ 28.5% lower than that of the tops. It

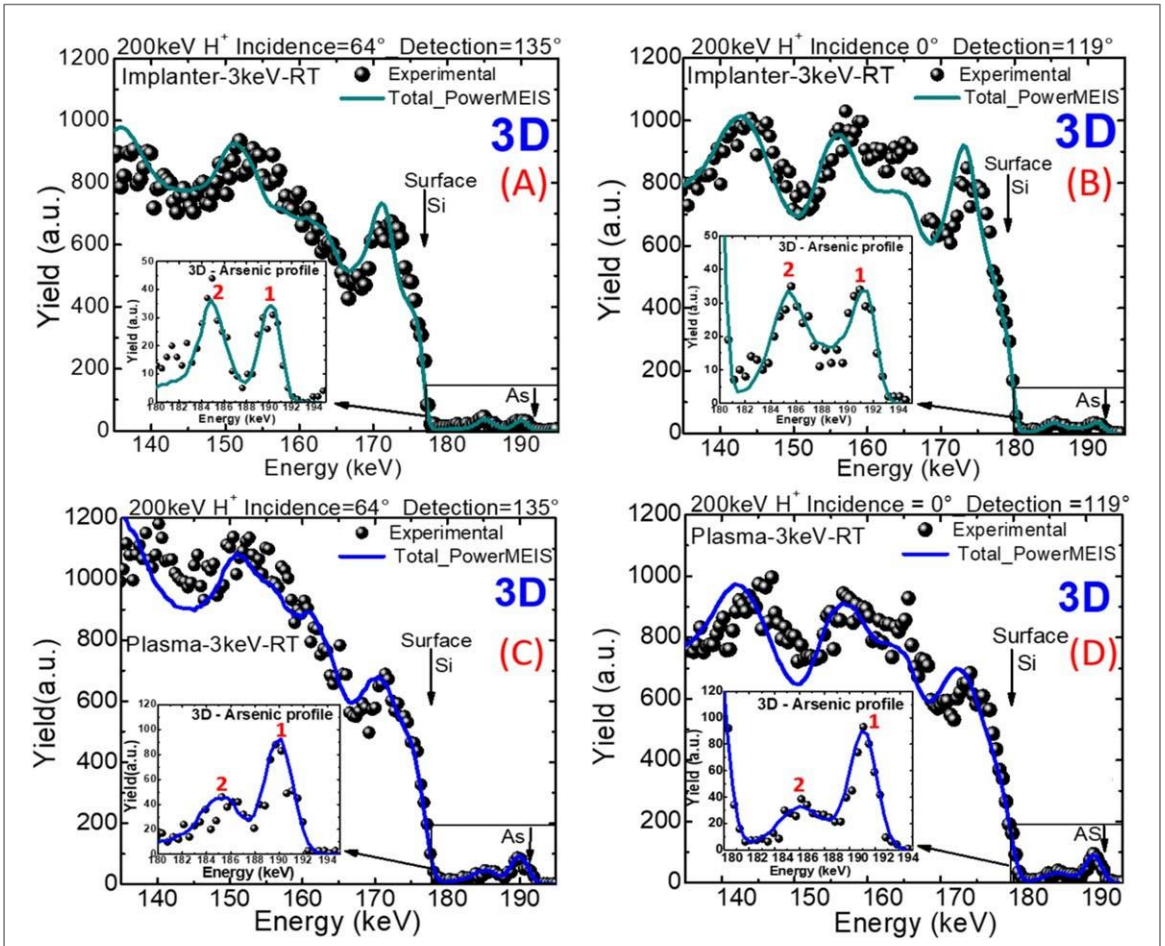


Figure 4. Experimental spectra with their associated PowerMEIS simulations, obtained on the nanostructured samples implanted by using the conventional method ((S1) - A and B) and plasma method ((S2) - C and D). The insets highlight the double peaks (1 and 2) of arsenic. The orientation of the lines grating was such that the scattered $H^+$ exit laterally with respect to the Fins.

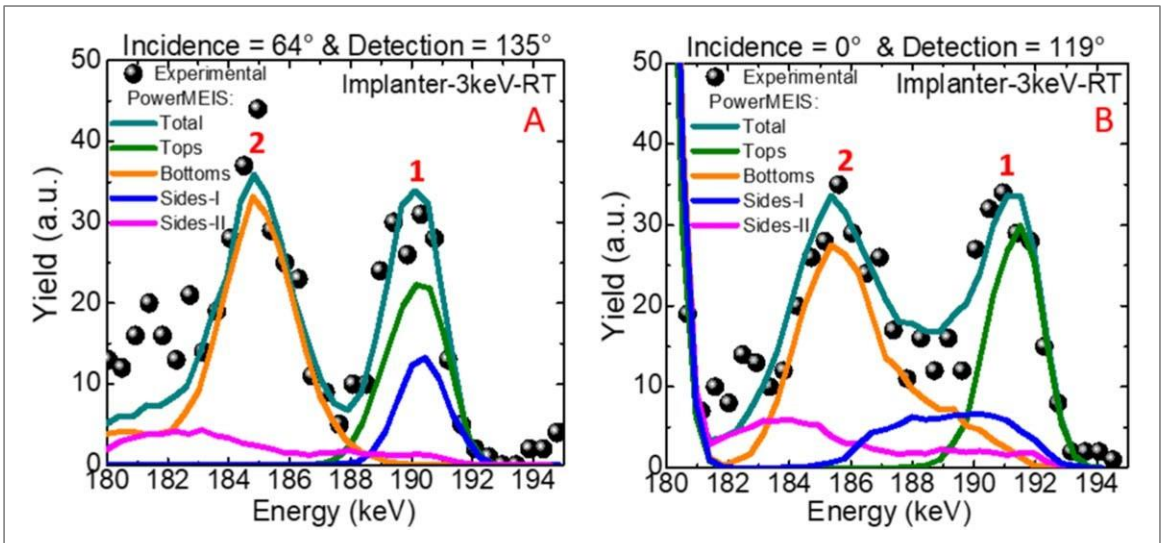


Figure 5. 3D deconvolutions of the arsenic spectra of each single part of the patterns of S1 by using PowerMEIS simulations.

should normally be higher as indicated in figure 6, if the implantation was conformal in S2. The intensities of the arsenic spectra in the sidewalls of S2 should be comparable to those of figure 6. These 3D deconvolutions show that the tops surface host a quantity of dopants larger than in the bottoms and sidewalls of S1 and S2. The chemical mapping carried out by energy dispersive x-ray (EDX) analyses on the two samples (figure 7) also show that the sidewalls are the least doped parts in conventional and plasma implantations. These images are in

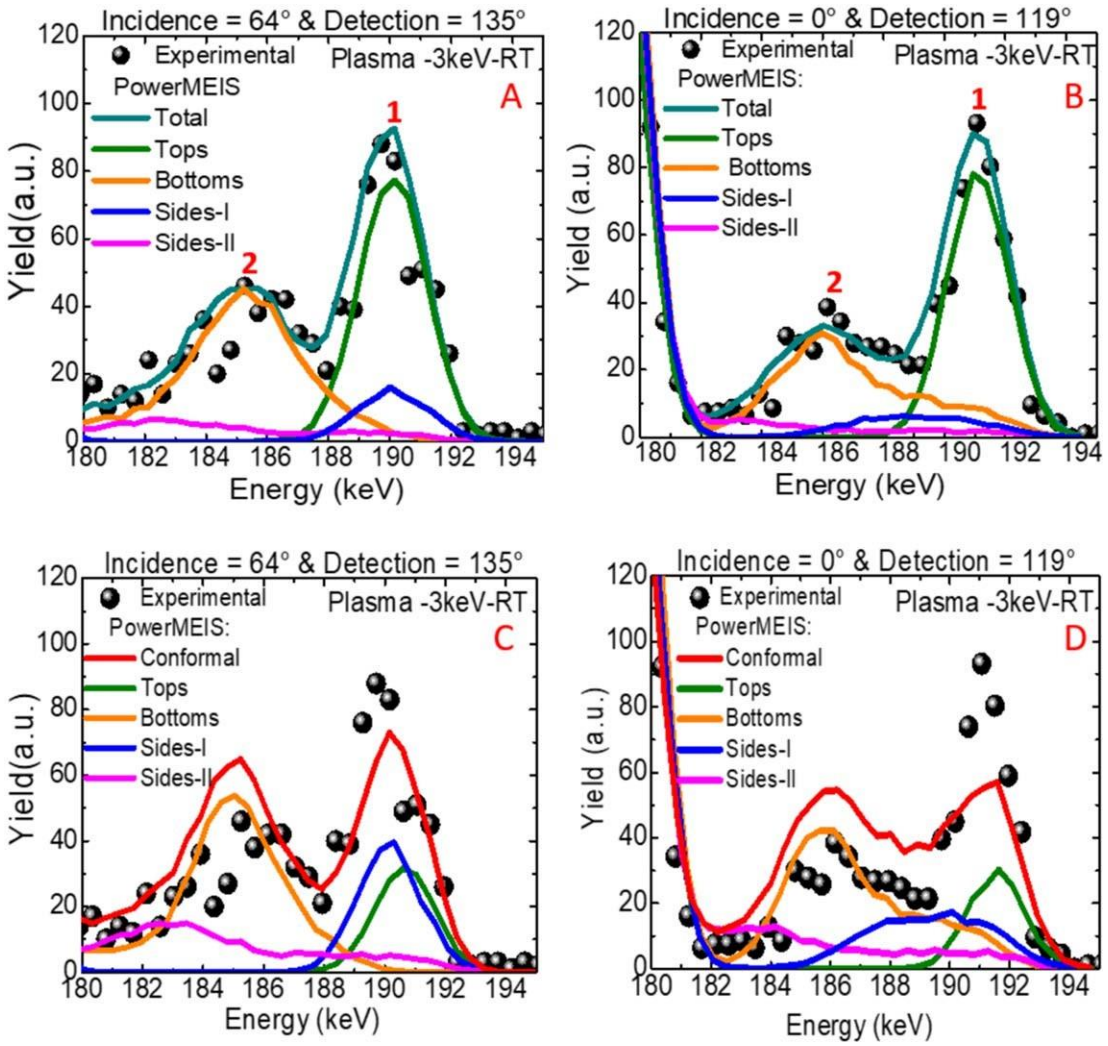


Figure 6. 3D deconvolutions of the arsenic spectra of each single part of the patterns of S2. The simulation of a conformal plasma implantation is illustrated in graphs C and D.

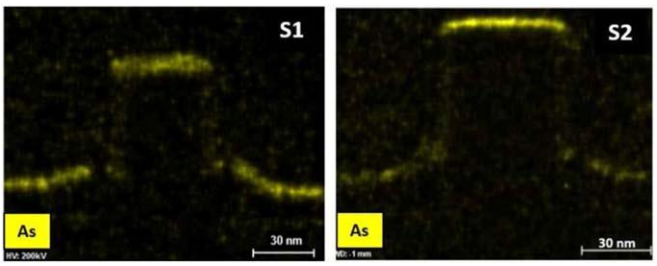


Figure 7. EDX image showing the chemical profile of arsenic (in yellow). S1: Implanter-3 keV-RT and S2: Plasma-3 keV-RT.

agreement with the spectra of figures 5 and 6 concerning the heavy doping of the top surfaces, and hence the non conformal distributions of implants.

Table 3 displays the local doses computed in the two 3D samples. They are normalized based on the measurements on their planar (non etched) areas. One can rely on the implantation conditions in the conventional method where the ions beam is unidirectional, to determine the expected local doses. This is not possible in plasma doping because of trajectories' distribution of the ions penetrating the materials surface. This method has thus permitted to compare the expected local doses in S1 with the measured ones and those determined by simulation of a conformal implantation. One can notice that the distribution of the measured dose in S1 is as expected. However, it is different from a conformal implantation because the sidewalls are less

Table 3. Comparison of the normalized local doses of arsenic in 3D samples (S1) and (S2). The values of the expected and conformal ones are determined by geometrical considerations and pure simulations, respectively.

| Normalized local doses of arsenic ($\times 10^{15}$at cm$^{-2}$), the uncertainty is in the order of $\pm$ 0.001. | | | |
|---|---|---|---|
| | Silicon Fins: | | |
| 3 keV—RT | Tops | Sidewalls (I+II) | Oxide Bottoms |
| Implanter (S1): | | | |
| expected | 1 | 0.23 | 0.76 |
| measured | 0.94 | 0.38 | 0.71 |
| conformal | 0.61 | 0.61 | 0.61 |
| Plasma (S2): | | | |
| measured | 1.95 | 0.24 | 0.45 |
| conformal | 0.62 | 0.62 | 0.62 |

doped ($0.38 \times 10^{15}$at cm$^{-2}$) than the tops ($0.94 \times 10^{15}$at cm$^{-2}$) and bottoms ($0.71 \times 10^{15}$at cm$^{-2}$). The distribution of the local dose implanted in S2 is also different from that of a conformal one. The measured dose in the tops ($1.95 \times 10^{15}$at cm$^{-2}$) is four times greater than that of the bottoms and eight times larger than in the sidewalls. This large concentration of dopants in the tops and the low sidewalls doping in plasma also illustrate that their distribution is different from that in conventional implantation as announced in figures 4 and 5. The explanations regarding the dicrepancies between the expected and targeted dose in 3D patterns of S2 and its distributions in each part can be as those provided for the planar one. The complex interactions between the energetic ions and neutrals, augmented to the 3D architecture and composition of the sample (Si and $SiO_2$) can explain the doping non conformity in plasma [12, 17, 21, 22]. There could also be a focusing effect of the ions on tops of the patterns implanted by plasma due to possible charge repulsions in the oxide. It was indeed reported in [23, 24] that a high fluence or high density $AsH_3^+$ plasma doping of an oxide can lead to charges accumulations. In this case, further investigations need to be carried out in the framework of future works as proposed in the conclusion. The observation of the possible arsenic loss by sublimation in a sample longly exposed to air is not excluded to explain the low bottoms doping in S2.

## 4. Conclusion

We were interested in studying 3D arsenic doping performed by plasma immersion ion and conventional implantations into SOI based Fin-shaped nanostructures for FinFETs manufacture. The analysis protocol has shown that the arsenic's spectrum does not display the same shape according to the geometry adopted for its measurement. The geometries chosen to investigate the 3D samples have been verified by the experiments. The analysis method that we have developed has permitted to highlight the contribution of the tops, sidewalls and bottoms in the construction of the overall spectra of arsenic. We have therefore discriminated the spectrum of the dopants implanted in the Si-Fins from that of the dopants implanted in the oxide. Rigorous analyses have served to demonstrate their non conformal distribution within the patterns, with non negligible discrepancies between the plasma and conventional implanter methods. The implantation performed with the conventional method in these studies displayed better results in terms of dopant distributions than with the plasma one. As future works proposed for the investigation of possible ion repulsions in the oxide, one may consider two nanostructures elaborated from the bulk silicon and SOI technologies. Then characterize the doping performed by one or the two above mentioned methods in the same conditions. Such studies could really be beneficial for the semiconductor community, namely for the SOI technology if they are correlated to molecular dynamic simulations.

## Acknowledgments

This work carried out on the Nano Characterization Plat-Form (PFNC) of CEA-Leti & Minatec european campus, was supported by the 'Recherches Technologiques de Base' Program of the French Ministry of Research. We are thankful to F. Mazen for providing the samples and to A. Jannaud for their preparation for microscopy analyses. The 3D simulations were performed via the PowerMEIS server of UFRGS in Brasil. Last,

we are also thankful to H. Guégan from ARCANE, the technology transfer unit of the Bordeaux—Gradignan Nuclear Research Center (CENBG) for RBS measurements.

## ORCID iDs

L Penlap Woguia https://orcid.org/0000-0003-0067-2694
F Pierre https://orcid.org/0000-0002-3021-3010
G G Marmitt https://orcid.org/0000-0002-8486-7001

## References

[1] Budrevicha A A and Vandervorst W 2016
[2] Chu P K, Chang N W C, Mizuno B and Monteiro O R 2000 *Hanbook of Plasma Immersion Ion Implantation and Deposition* (605 Third Avenue New York: Wiley) 99-89627
[3] England J, Möller W, van den Berg J, Rossall A, Min W and Kim J 2017 *Nucl. Instrum. Methods Phys. Res.* B60–4 URL https://doi.org/10.1016/j.nimb.2017.05.043
[4] Demenev E, Giubertoni D, van den Berg J, Reading M and Bersani M 2012 *Nucl. Instrum. Methods Phys. Res., Sect. B* 273 192–4 XX International Conf. on Ion Beam Analysis
[5] Min W J, Kim J, Park K, Marmitt G, England J and Moon D W 2019 *Anal. Chem.* 9315–22
[6] England J, dos Santos Rosa L, Min W J and Kim J 2018 Tri3dyn modelling and medium energy ion scattering measurements of as dopant profiles in finfets *XXII International Conf. on Ion Implantation Technology (IIT 2018)* p 137
[7] Werner M, Van den Berg J A, Armour D G, Vandervorst W, Collart E, Goldberg R, Bailey P and Noakes T C Q 2004 *Nucl. Instrum. Methods Phys. Res.* B 214 67–74
[8] Cullis A, Seidel T and Meek R 1978 *J. Appl. Phys.* 49 5188–98
[9] Dalponte M, Boudinov H, Goncharova L V, Garfunkel E and Gustafsson T 2007 *J. Phys. D: Appl. Phys.* 40 4222-7
[10] Lieberman M A and Lichtenberg A J 2005 *Principles of Plasma Discharges and Materials Processing* (New York: Wiley)
[11] Chu W K, Mayer J W and Nicolet M A 1978 *Basckattering Spectrometry* (UK: Harcourt Barce Jovanovich, Publishers)
[12] Jalabert D, Vickridge I and Chabli A 2017 *Swift Ion Beam Analysis in Nanosciences* (Willey) URL http://www.willey.com
[13] Gemmell D S 1974 *Rev. Mod. Phys.* 46 129–227
[14] Sortica M A, Grande P L, Machado G and Miotti L 2009 *J. Appl. Phys.* 106 114320
[15] UFRGS 2010 *PowerMEIS 2.0 User's Manual* 2 1–20
[16] Sanchez D F, Marmitt G G, Marin C, Baptista D L, Azevedo G M, Grande P L and Fichtner P F P 2013 *Sci. Rep.* 3 3414
[17] Trombini H *et al* 2019 *Sci. Rep.* 9 11629 https://doi.org/10.1038/s41598-019-48117-0
[18] Laricchiuta G, Vandervorst W, Vickridge I, Mayer M and Meersschaut J 2019 *Journal of Vacuum Science & Technology* 37 020601 https://doi.org/10.1116/1.5079520
[19] Mayer M *SIMNRA User's Guide Max-Planck-Institut für Plasmaphysik* URL http://www.simnra.com
[20] Zalm P, Bailey P, Reading M, Rossall A and den Berg J A V 2016 *Nucl. Instrum. Methods Phys. Res.* B 396 160–4
[21] England J, den Berg J V and Rossall A 2019 *Journal of Vacuum Science & Technology B* 37 031206 https://doi.org/10.1116/1.5088958
[22] Anders A 2000 *Handbook of Plasma Immersion Ion Implantation and Deposition* (USA: Wiley-Interscience Publication)
[23] Qin S, Bernstein J D, Zhao Z, Liu W and Chan C 1995 *J. Vac. Sci. Technol.,* B 13 1994–8
[24] Chu P K 2004 *J. Vac. Sci. Technol.* B 22 289–96